Article

Computational Investigation of the Thermochemistry of the CO_2 Capture Reaction by Ethylamine, Propylamine, and Butylamine in Aqueous Solution Considering the Full Conformational Space via Boltzmann Statistics

Joseph Schell, Kaidi Yang, and Rainer Glaser*

ACCESS | Metrics & More | Article Recommendations | Supporting Information

ABSTRACT: Rubisco is the enzyme responsible for CO_2 fixation in nature, and it is activated by CO_2 addition to the amine group of its lysine 201 side chain. We are designing rubisco-based biomimetic systems for reversible CO_2 capture from ambient air. The oligopeptide biomimetic capture systems are employed in aqueous solution. To provide a solid foundation for the experimental solution-phase studies of the CO_2 capture reaction, we report here the results of computational studies of the thermodynamics of CO_2 capture by small alkylamines in aqueous solution. We studied CO_2 addition to methyl-, ethyl-, propyl-, and butylamine with the consideration of the full conformational space for the amine and the corresponding carbamic acids and with the

application of an accurate solvation model for the potential energy surface analyses. The reaction energies of the carbamylation reactions were determined based on just the most stable structures (MSS) and based on the ensemble energies computed with the Boltzmann distribution (BD), and it is found that $\Delta G_{BD} \approx \Delta G_{MSS}$. The effect of the proper accounting for the molecular translational entropies in solution with the Wertz approach are much more significant, and the free energy of the capture reactions $\Delta^W G_{BD}$ is more negative by 2.9 kcal/mol. Further accounting for volume effects in solution results in our best estimates for the reaction energies of the carbamylation reactions of $\Delta^W A_{BD} = -5.4$ kcal/mol. The overall difference is $\Delta G_{BD} - \Delta^W A_{BD} = 2.4$ kcal/mol for butylamine carbamylation. The full conformational space analyses inform about the conformational isomerizations of carbamic acids, and we determined the relevant rotational profiles and their transition-state structures. Our detailed studies emphasize that, more generally, solution-phase reaction energies should be evaluated with the Helmholtz free energy and can be affected substantially by solution effects on translational entropies.
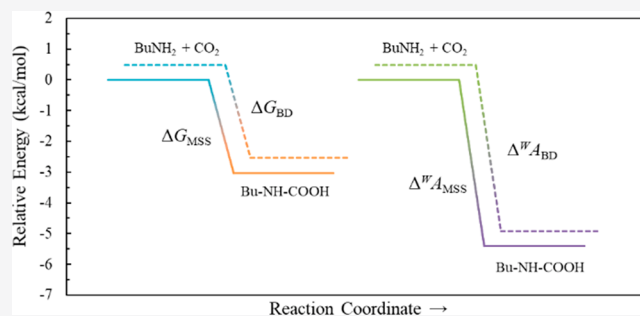
1. INTRODUCTION

As of January 2021, the global concentration of CO_2 in the atmosphere has reached 415.13 ppm,[1] and there has been no slowing of the rate of atmospheric CO_2 increase (∼15 ppm/decade). Drastic cutbacks of CO_2 emissions and more complete CO_2 capture at concentrated sources and current negative emissions technologies[2−7] will not be sufficient to reverse trends. Even at current atmospheric CO_2 levels, it will not be possible to halt global climate change because natural CO_2 capture is a slow process.[8,9] Thus, there is a clear need for the development of new methodologies for CO_2 capture of carbon dioxide from ambient air.[10,11] Amine-based CO_2 capture has been widely studied, and aqueous amines are by far the most common systems used for capturing CO_2 at concentrated sources.[12,13]

The energy required to release CO_2 after its capture is the limiting factor for large-scale CO_2 extraction using capture-and-release systems.[14,15] To minimize this high cost, we have

been interested in CO_2 direct air capture (DAC),[16−18] and we have been studying the rubisco-based biomimetic system for such a purpose.[19−21] Ribulose-1,5-bisphosphate carboxylase/oxygenase (rubisco) is the enzyme responsible for most of the fixation of CO_2 from air.[22] The active site of spinach rubisco (1AUS, Scheme 1) contains the amine group of the side chain of Lys201 and a hydrated magnesium ion that is held in place by the carboxylic acid groups of Asp203 and Glu204.[23] In order to accomplish its enzymatic activity, Lys201 must be activated via carbamylation of the nitrogen in the side chain.[24,25] We suggest that this carbamylation reaction is a
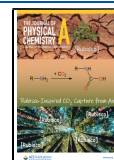
Scheme 1. From Rubisco to Tetrapeptide to Butylamine
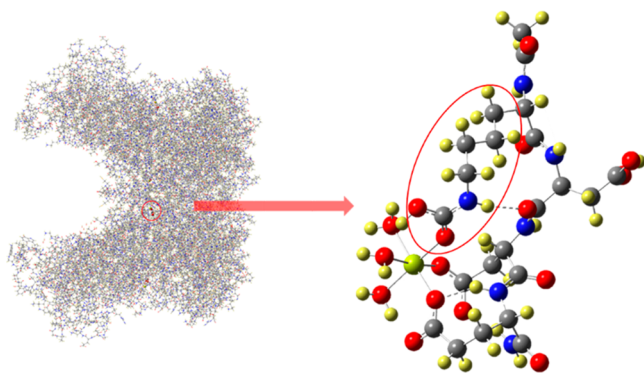
suitable capture-and-release system (CRS) and that the Mg^{2+}-complexed tetrapeptide KDDE (Scheme 1) presents the smallest chemical implementation of a CRS that may replicate the chemical environment of the enzyme. Computational studies of KDDE models[19,20] have suggested that it would be a good candidate for a capture-and-release system because the thermodynamics of the capture mechanism allow for the reaction spontaneity to be readily controlled with temperature. Ideally, the capture of CO_2 by the CRS will be spontaneous at a reasonable reaction temperature, and the reverse reaction, CO_2 release, will be spontaneous at moderately higher temperature conditions. In other words, the equilibrium of the reaction is heavily influenced by the entropy term such that the CRS can be controlled with moderate temperature

changes. In fact, an ideal capture reaction will be both modestly exergonic for efficient loading and highly exentropic for efficient removal of CO_2. We have been measuring the thermodynamics of the CO_2 capture by the KDDE tetrapeptide in the presence and absence of Mg^{2+} ions and as a function of pH. To discern the importance of the Mg^{2+} complexation, it became necessary to study CO_2 capture by the lysine side chain itself. Research in our group aims to determine the ΔG value of the capture reactions. The extraction of the desired ΔG value from the experimental measurements of the carbamylating reactions relies on the acidity constants of carbonic acid, bicarbonate, carbamic acid, and the conjugate acid of the amine. All of these equilibrium constants are associated with uncertainties and complicate the experimental determination of ΔG of the capture reaction. In this context, it is crucial to provide the very best possible computational estimate of the carbamylating reaction.

Here, we report the results of computational studies of the thermodynamics of CO_2 capture by small alkylamines in aqueous solution. Specifically, we studied CO_2 addition to methylamine **Me-1**, ethylamine **Et-1**, propylamine **Pr-1**, and butylamine **Bu-1** at room temperature with consideration of the full conformational space for the amine **R-1** and the corresponding carbamic acids **R-2** and **R-3** (Scheme 2, top row). **R-2** and **R-3** are the *trans* ($\alpha = 180°$) and *cis* ($\alpha = 0°$) carbamic acids, respectively. We also studied two conformational face change processes of the most stable conformers in **R-2**. The first one involves the rotation around the N−C1 bond, described by dihedral angle $\chi = \angle(HO_2C-N-C1-C2)$. This process changes the position of the carboxylic acid group

Scheme 2. Alkylamines (AM) and Alkylcarbamic Acids (CA) and the Interconversion between Enantiomeric Conformers and Isomerization Were Studied for R = Me, Et, Pr, and Bu
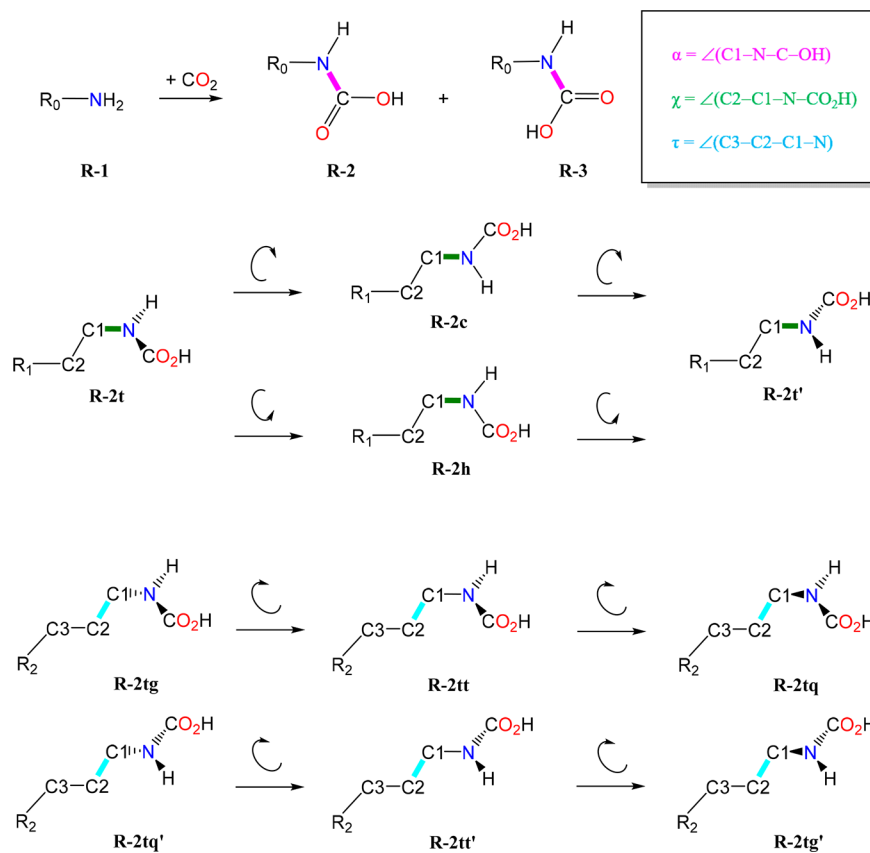
relative to C1−C2−R$_1$ plane and leads to the interconversion between enantiomeric conformers **R-2t** and **R-2t′** (Scheme 2, middle row) with two rotational directions. The second face change process is particularly important in Rubisco and involves the rotation around the C1−C2 bond, described by the dihedral angle $\tau = \angle(N-C1-C2-C3)$, and moves the entire carbamic acid function group from one face of the C1−C2−C3 plane to the other (Scheme 2, bottom rows).

The common procedure for the calculation of reaction energies involves the energies of the most stable structure (MSS) of each species involved in the reaction, and we will show those results. In addition, and to achieve more accurate results, we also determined the reaction thermodynamics based on the Boltzmann average of the Gibbs free energy over all of the conformers. This undertaking presents significant challenges, and these include (a) the consideration of all possible conformations, (b) the possible degeneracy of chiral structures, and (c) the determination as to whether a stationary structure contributes to the Boltzmann analysis. Scheme 3 shows all

Scheme 3. Non-eclipsed Structures of C−N Conformers of a RCH$_2$−N(sp^2)HX System
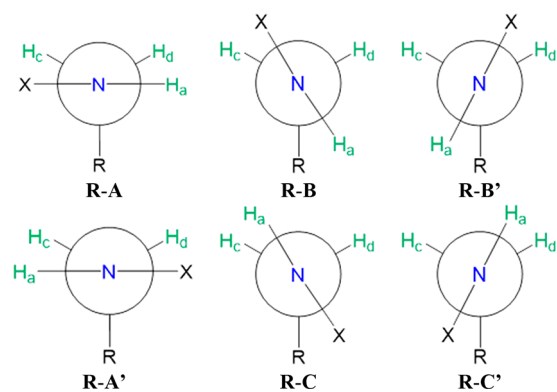
possible non-eclipsed structures for a RCH$_2$−N(sp^2)H−X system. If the R group is achiral, then R-A and R-A′, R-B and R-B′, and R-C and R-C′ are enantiomeric conformers, and if R is chiral, then these pairs are epimeric conformers. Table 1 aids

Table 1. Enumeration of Unique Trial Structures and Minima

molecule and type	number of unique trial structures	number of unique, asym. local minima located	number of unique, sym. local minima located	number of local minima used in Boltzmann analysis N$_{total}$
Me-1			1	1
Me-2			1	1
Me-3			1	1
Et-1	2	1	1	3
Et-2	3	2^a	0	2
Et-3	3	2^a	0	2
Pr-1	5	4	1	9
Pr-2	9	4	0	8
Pr-3	9	4	1^a	8
Bu-1	14	13	1	27
Bu-2	27	11	1^a	22
Bu-3	27	13	1^a	26

^{a}Includes a local minimum on the potential energy surface but not counted in population analysis; see text.

in the enumeration of the stationary structures, and it shows, for example, that 48 out of 54 possible local minima need to be considered for butylcarbamic acid. Importantly, we will show several cases where the unusual characteristics of the rotational profile about the RCH$_2$−NHCO$_2$H dihedral angle (χ scans) have nonintuitive effects on the Boltzmann analysis.

2. COMPUTATIONAL METHODS

Structure optimizations and analytical frequency calculations were performed using Gaussian16[26] using the APFD density functional[27] and the polarized triply split valence basis set 6-311G*.[28−30] Implicit water solvation was incorporated via the solvation model based on solute electron density (SMD).[31] The APFD density functional was developed with special consideration of structure and bonding of organic molecules, and the method accounts well for intramolecular dispersion.[27] This functional has acquired a proven performance record in comparative evaluations.[32,33] In our own work, we achieved good agreement between computations at this level and experimental measurements. A brief discussion of theoretical level dependencies with focus on N-pyramidalization is provided in the Supporting Information. Our choice of basis set is a compromise between size and computational demand. The literature suggests that the 6-311G* basis set is large enough to avoid significant effects on the energies of the carbamylation reactions caused by basis set superposition error[34] (BSSE), and intramolecular BSSE values are estimated to be only about 0.1 kcal/mol.[35]

For each unique amine structure, we report in Table 2 the total energy (E, in a.u.), vibrational zero-point energy (VZPE, in kcal/mol), thermal energy (TE, in kcal/mol), and molecular entropy (S, in cal mol^{-1} K^{-1}). The same information is reported in Table S2 for all conformers of the carbamic acids for the methyl, ethyl, propyl, and butyl systems.

For molecules with several stereoisomers, we also report their relative stabilities ΔG_{rel} (in kcal/mol) relative to the most stable stereoisomer. Based on the calculated relative energies ΔG_{rel}, we determined their individual contributions at $T = 298.15$ K using the Boltzmann distribution (eq 1).

$$f_i = \frac{N_i}{N_{total}} = \frac{e^{(-G_i/RT)}}{\sum_{j=1}^{N_{total}} e^{-G_j/RT}} \tag{1}$$

The evaluation of the Boltzmann-averaged Gibbs free energies requires the knowledge of the stabilities G_j of all possible stereoisomers (N_{total}) and the population fraction $f_i = N_i/N_{total}$ for a given stereoisomer i calculated via eq 1. The population of each stereoisomer, $P_i = N_i/N_{total} \times 100\%$, is reported as a percentage in the last column of Table 2 for the amines and in the last column of Table S2 for the carbamic acids.

For the capture reaction AM + CO$_2$ → CA, the reaction free energy ΔG is determined as the difference between the sums of the free energies of products and starting materials. The fastest approximation is based on the evaluation of the reaction energy using the most stable structure of each species, S, and we will call this ΔG_{MSS}(S). A better approximation to the reaction free energy considers the average energy of each species based on the populations and stabilities of its isomers, ΔG_{BD}(S). Equation 2 is used to determine the free energy of any given molecule as a sum of the free energies of each conformer. However, these free energies are more intuitive

Table 2. Thermodynamic Properties and Relative Energies[a,b] for All Amine Conformers

species	energy	VZPE	TE	S	ΔE_{rel}	ΔG_{rel}	P_i
CO$_2$	−188.486130	7.31	8.96	51.08		0.00	100.0
methylamine							
Me-1	−95.797578	40.67	42.79	57.23		0.00	100.0
ethylamine							
Et-1t	−135.090187	58.51	61.32	65.41	0.00	0.00	73.9
Et-1g (2)	−135.088981	58.64	61.36	64.65	0.76	1.03	13.1
propylamine							
Pr-1tg (2)	−174.379037	76.65	80.10	71.89	-0.09	0.07	23.7
Pr-1tt	−174.378888	76.55	80.08	72.37	0.00	0.00	26.7
Pr-1gg (2)	−174.377422	76.73	80.16	71.77	0.92	1.18	3.6
Pr-1gt (2)	−174.377635	76.63	80.13	72.22	0.79	0.89	6.0
Pr-1gq (2)	−174.376938	76.57	80.07	72.35	1.22	1.23	3.4
butylamine							
Bu-1tgg (2)	−213.667383	94.75	98.93	78.86	0.12	0.41	7.7
Bu-1tgt (2)	−213.667580	94.57	98.83	79.51	0.00	0.00	15.5
Bu-1tgq (2)	−213.664572	94.88	99.02	78.36	1.89	2.42	0.3
Bu-1ttg (2)	−213.666499	94.63	98.91	79.79	0.68	0.67	5.0
Bu-1ttt	−213.667383	94.53	98.87	79.97	0.12	0.02	15.0
Bu-1ggg (2)	−213.665782	94.85	98.99	78.37	1.13	1.63	1.0
Bu-1ggt (2)	−213.666025	94.65	98.90	79.26	0.98	1.11	2.4
Bu-1ggq (2)	−213.663194	94.70	98.90	78.97	2.75	2.98	0.1
Bu-1gtg (2)	−213.665511	94.66	98.91	79.44	1.30	1.40	1.5
Bu-1gtt (2)	−213.666171	94.55	98.87	79.81	0.88	0.83	3.8
Bu-1gtq (2)	−213.665135	94.58	98.89	80.19	1.53	1.39	1.5
Bu-1gqg (2)	−213.662641	94.61	98.85	79.65	3.10	3.08	0.1
Bu-1gqt (2)	−213.665543	94.45	98.77	80.12	1.28	1.03	2.7
Bu-1gqq (2)	−213.665219	94.68	98.89	79.25	1.48	1.62	1.0

[a]All values determined at SMD(APFD/6-311G*). [b]E in Hartree, TE in kcal/mol, S in cal mol^{-1} K^{-1}, ΔG_{rel} in kcal/mol, and P_i is the percentage population of that conformer according to the Boltzmann statistics. A "(2)" behind the conformer descriptor indicates that the structure has an enantiomeric conformer, which is included in the Boltzmann statistics.

when reported relative to the most stable structure, and eq 2 can be adapted to eq 3.

$$\langle G \rangle = \sum_{i=1}^{N_{total}} f_i G_i \tag{2}$$

$$\langle G_{rel} \rangle = \sum_{i=1}^{N_{total}} f_i G_{rel,i} \tag{3}$$

The calculation of the free energies of reaction are then given by eqs 4−6. Equation 4 is the traditional approach, using only the free energies of the most stable structures of the products and reagents. Equation 6 accounts for the contribution to the reaction free energy from the other conformers.

$$\Delta G_{MSS} = G(CA_{MSS}) - G(AM_{MSS}) - G(CO_2) \tag{4}$$

$$\Delta G_{BD} = \langle G(CA) \rangle - \langle G(AM) \rangle - G(CO_2) \tag{5}$$

$$\Delta G_{BD} = \Delta G_{MSS} + \langle G_{rel}(CA) \rangle - \langle G_{rel}(AM) \rangle \tag{6}$$

The same equations apply to the Helmholtz free energy, ΔA, of the reactions. By definition, $\Delta G = \Delta A + \Delta(pV)$. The pV term is important in gas-phase thermochemistry. For ideal gas behavior $\Delta(pV) = \Delta n(RT)$ at room temperature and $\Delta G = \Delta A - 0.593$ kcal/mol. However, in condensed phase, $\Delta(pV) \approx 0$ because the expansion of the solution is almost negligible. Therefore, the calculated Gibbs free energy is likely over-estimated, and the ΔA value is a better estimate of the reaction energy in the condensed phase. For this reason, the Helmholtz

free energies will be reported alongside the Gibbs free energies in tables describing reaction thermochemistry.

$$^wS_{trans} = 0.54S_{trans} + 6.578 \tag{7}$$

Various corrections have been proposed to better estimate the reaction thermodynamics of condensed phase systems based on their gas-phase energies. The Wertz[36] correction in eq 7 is one such estimate empirically derived from the comparison of measured and computed solvation energies of various compounds in water. We apply this correction to the calculated translational entropy for each molecule because the translational component is the most affected by the transition from gas phase to solution. The Wertz-corrected free energy values are also given in all tables describing reaction thermochemistry.

3. RESULTS AND DISCUSSION

3.1. Enumeration of Conformations of Ethylamine and *N*-Ethylcarbamic Acid. *3.1.1. Possible Structures.* The parent alkyl systems, the methyl systems, are trivial in that only one conformation occurs for each of **Me-1**, **Me-2**, and **Me-3** (Figure S2). More options exist for the ethyl systems. Newman projections along the N−C1 bond of the expected conformations of ethylamine **Et-1** and of ethylcarbamic acids **Et-2/Et-3** are shown in Scheme 4. Throughout, we chose to orient the C1−C2 bond as shown in Scheme 4. Molecular models of the optimized structures of ethylamine and of ethylcarbamic acid are shown in Figure 1.

Scheme 4. Trial Conformations of Ethylamine and Ethylcarbamic Acid
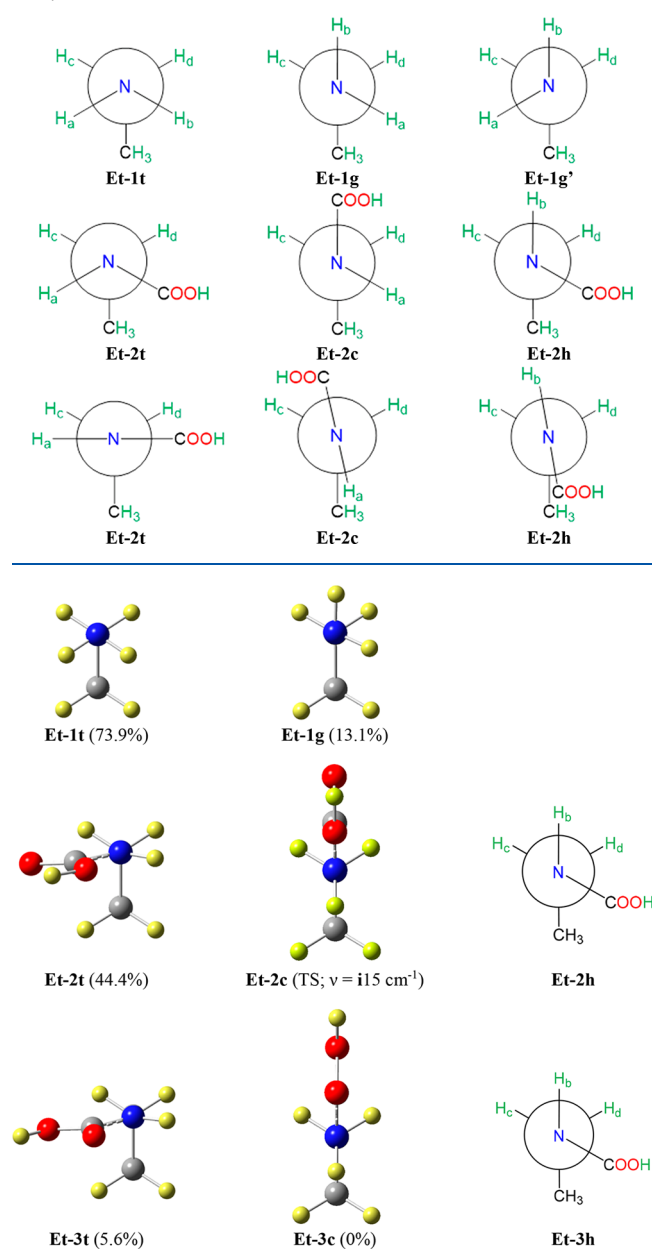
Figure 1. Optimized structures of unique conformers of ethylamine. Newman projections are shown with respect to the N−C1 bond. The number in parentheses is the population percentage in the Boltzmann analysis at 298 K for a single unique enantiomeric conformer. **Et-2t** and its enantiomeric conformer **Et-2t′** are dominating with a combined population of 88.8%. The *cis* arrangement of the methyl and carboxyl group is strictly avoided and optimization of trial structures of **h**-type result in **t**-type structures.

The conformers **Et-1t** and **Et-1g** differ in the orientation of the N lone pair. Each conformation can be described by one of two dihedral angles $\eta_a = \angle(H_a-N-C1-C2)$ and $\eta_b = \angle(H_b-N-C1-C2)$. To facilitate the discussion, we will simply refer to these two conformations as **t** and **g** depending as to whether the N lone pair is *trans* or *gauche* with respect to the C1−C2 bond (τ_1). There are, of course, two *gauche* conformations, **g** and **g′** (the enantiomeric conformer of **g**), and both of these will matter in the Boltzmann statistical analysis (vide infra).

Here, we do show both **Et-1g** and **Et-1g′**, but in the structural discussions below, we will consider only one unique structure of any pair of enantiomeric conformers, and these will usually be analogues of **Et-1g**.

The conformers of ethylcarbamic acid **Et-2t**, **Et-2c**, and **Et-2h** differ in the position of the COOH group. Formally, **Et-2t** results by replacement of H_b in **Et-1t** by the COOH group. Of course, one could also replace H_a with COOH and generate the enantiomeric conformer **Et-2t′** (not shown for brevity). Structures **Et-2c** and **Et-2h** result by replacement of H_b or H_a in **Et-1g**, respectively, and the names reflect whether the N−$\underline{C}$OOH bond or the remaining N−$\underline{H}$ bond is in a *trans* position relative to the C1−C2 bond. As always, **Et-2c′** and **Et-2h′** refer to the enantiomeric structures. The carbamic acids usually are trigonal planar about the N atom, and the Newman projections shown in the bottom row of Scheme 4 are more appropriate. For structures of type **Et-2t**, the N-planarization does not cause any eclipsing, while structures of types **Et-2c** and **Et-2h** inadvertently would contain one near-eclipsed conformation. In other words, such structures will have a driving force to at least some degree of N-pyramidalization to avoid such eclipsing as much as possible. For this reason, the schematic Newman projections shown in the second row are advantageous for the enumeration of the *complete* conformational space, and they will be used in the subsequent discussions of the larger alkylcarbamic acid structures.

As shown in the top row of Scheme 2, the carbamylation reaction can form two geometric isomers regarding the carbamic acid. The *trans*-amide **2** is generally preferred over the *cis*-isomer **3**. Both species were investigated in every case. The equilibration between **2** and **3** does not require rotation about the N−CO₂H bond but can be accomplished very fast by proton transfer. Therefore, the Boltzmann statistical population analysis was performed on the set of all carbamic acid structures rather than on the subsets of structures **2** and **3**.

3.1.2. Models of Local Minima Ethylamine and N-Ethylcarbamic Acid. Molecular models of all the optimized structures of ethylamine and ethylcarbamic acid are shown in Figure 1. Here and elsewhere, we show the schematic Newman projection of any conformation that was considered as an initial trial structure but did not correspond to a stationary structure on the respective potential energy surface. For **2** and **3**, we were able to locate two conformers while all attempts to locate **Et-2h** or **Et-3h** led to one of the existing stationary structures. In Table S2, we include one row for every expected carbamic acid structure and explicitly indicate if such an expected structure does not exist.

The energies and relative stabilities of ethylamine are listed in Table 2. **Et-1t** is a C_s-symmetric structure, and it is unique. On the other hand, **Et-1g** is an asymmetric structure, and so there also exists its enantiomeric conformer **Et-1g′**. Table 2 contains one row for such a set of enantiomeric conformers, and the number of symmetry-related stationary structures is indicated in parentheses following the structure descriptor.

The preferred conformation of ethylamine in the gas phase was determined by microwave spectroscopy,[37] and it is **Et-1t** and the same is true in aqueous solution. The preferred conformation of ethylcarbamic acid is **Et-2t**; that is, the *trans*-amide geometry is greatly preferred in the carbamic acid context compared the respective *cis*-amide **Et-3t**. We also find a *trans*-amide preference for the pair **Et-2c** and **Et-3c**.

3.1.3. Potential Energy Surface for EtNH−COOH Torsion. There is the possibility for C_s-symmetry for **Et-2c** and **Et-3c**. A
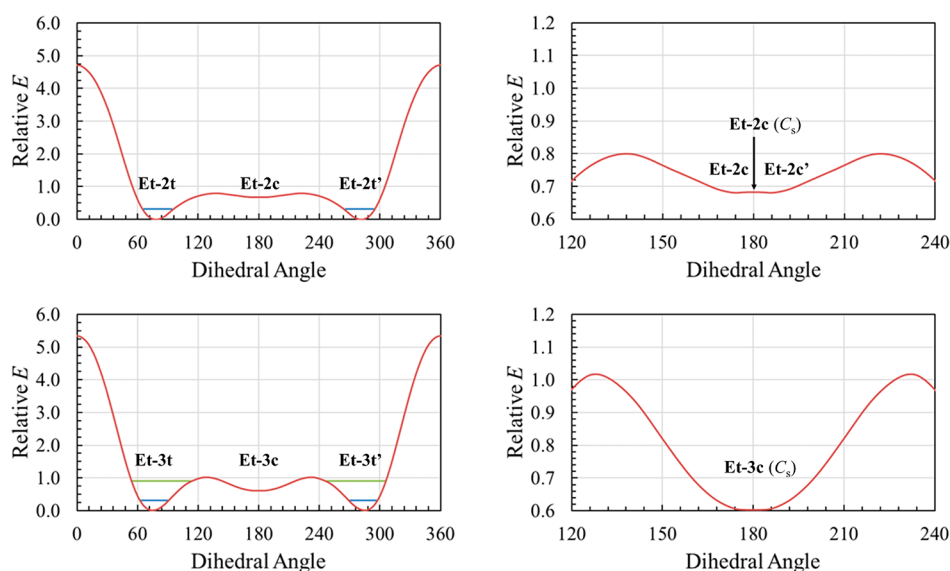
Figure 2. PES scans of the dihedral angle $\chi = \angle(HO_2C-N-C1-C2)$ for ethylcarbamic acids **Et-2** and **Et-3**. Plots on the left show the full χ range, and plots on the right are close-ups of the regions containing **Et-2c** and **Et-3c**, respectively. Relative energy E in kcal/mol. The horizontal lines indicate bound vibrational levels. None of the **c**-type structures correspond to bound states. Interconversion between enantiomeric conformers is very fast via the **c**-type structures and much faster compared to the path via the **h**-type structures ($\chi = [0°, 360°]$).

scan of the dihedral angle $\chi = \angle(HO_2C-N-C1-C2)$ of both **Et-2** and **Et-3** is shown in Figure 2, and we first discuss the situation for **Et-3**.

The C_s-symmetric structure **Et-3c** is a local minimum on the PES but a very shallow one ($\nu_1 = 29$ cm^{-1}). A scan in the vicinity of **Et-3c** as a function of the dihedral χ shows that the barrier to rotation about the N−C1 bond is merely $\Delta E = 0.470$ kcal/mol and lower than the thermal energy associated with the ν_1 mode of C_s-**Et-3c** (0.593 kcal/mol). Thus, C_s-**Et-3c** does *not* correspond to local minimum; instead, it is an *unbound minimum* (UBM) and not considered in the Boltzmann analysis. Essentially, the entire **Et-3c** region is a transition-state region for the interconversion between enantiomeric conformers **Et-3t** ⇌ **Et-3t**′. The situation for **Et-2** is qualitatively similar except that the sink for **Et-2c** is even more shallow than it is for **Et-3c**. The top-right panel of Figure 2 shows that the **Et-2c** region is very flat and contains a C_s-symmetric transition-state structure ($\nu_1 = $ i15 cm^{-1}) between a pair of C_1 minima. Structures of the type **Et-2c** are UBMs, and essentially, the entire **Et-2c** region is a transition-state region for the interconversion between enantiomeric conformers **Et-2t** ⇌ **Et-2t**′.

The sinks around **Et-3t** and its enantiomeric conformer are shallow, containing at most two bound vibrational states for the normal mode promoting the rotation about the C1−N bond ($\nu_2 = 108$ cm^{-1}). The sinks around **Et-2t** and **Et-2t**′ are even more shallow and contain only one bound vibrational state for the normal mode promoting the rotation about the C1−N bond ($\nu_2 = 108$ cm^{-1}). Therefore, **Et-3** is a fluxional molecule with equal populations of **Et-3t** and **Et-3t**′, and **Et-2** is a highly fluxional molecule with equal populations of **Et-2t** and **Et-2t**′.

3.1.4. Relative Energies and Population Analysis. The number of species entering the Boltzmann statistical analysis is listed in Table 1. For the ethylamine species, there were only three structures: **Et-1t**, **Et-1g**, and **Et-1g**′. At room temperature, **Et-1t** was more favorable than the *gauche* conformers by 1.03 kcal/mol, and therefore, 73.9% of the molecules exist in

this conformation at any given time. Thus, 26.1% of the ethylamine molecules will exist in either one of the two *gauche* conformations. The ethylcarbamic acids were treated as a single set in the Boltzmann analysis. Because the **Et-Xh** conformers could not be located as local minima, they are not included in the statistical analysis. The transition-state **Et-2c** and the unbound minimum **Et-3c** are also not included in the statistical analysis. Therefore, only the asymmetric **Et-2t** and **Et-3t** and their enantiomeric conformers are included in the Boltzmann analysis, for a total of four species. The *trans*-amides are more favorable than the *cis* analogues by 1.22 kcal/mol, and they have significantly more contribution to the overall population at room temperature. **Et-2t** and **Et-2t**′ combined account for 88.7% of the overall population of ethylcarbamic acid at room temperature and the remaining 11.3% is split between the two *cis* conformers.

Table 3 lists the Gibbs free energies of the most stable structures of ethylamine and ethylcarbamic acid: **Et-1t** and **Et-2t**. It also lists the average Gibbs free energy $\langle G_{298} \rangle$ for those species calculated using all of the conformers and their population fractions, based on eqs 1 and 2. The difference $\langle G_{rel} \rangle$ between the averaged free energy and the free energy of the most stable structure is given in the final column in kcal/mol. Based on these values and the free energy of CO_2, the reaction energies were calculated for the CO_2 capture reaction by ethylamine and appear in Table 4. In the case of the most stable structures, the capture reaction free energy would be the ΔG for reaction R1.

$$\textbf{Et-1t} + CO_2 \rightarrow \textbf{Et-2t} \qquad \qquad (R1)$$
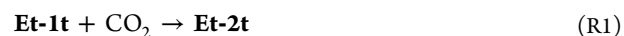
When using the Boltzmann-averaged energy values, the ΔG_{BD} reflects the energy difference between the average molecular energy of an ethylcarbamic acid molecule and the energy of the average ethylamine molecule. The Helmholtz free energies for the capture process are also provided in Table 4 for the reasons discussed above.

3.2. Enumeration Conformations of Propylamine and Propylcarbamic Acid. *3.2.1. Possible Structures.* We

Table 3. Calculated Thermodynamic Values for the Species Involved in Carbamylation Reaction[a,b]

molecule	MSS approach		BD approach	
	G_{298}	MSS	$\langle G_{298}\rangle$	$\langle G_{rel}\rangle$
CO$_2$	−188.495174			
methylamine	−95.755642	**Me-1**		0.00
methylcarbamic acid	−284.256655	**Me-2**	−284.256453	0.13
ethylamine	−135.022601	**Et-1t**	−135.022175	0.27
ethylcarbamic acid	−323.521874	**Et-2t**	−323.521655	0.14
propylamine	−174.284721	**Pr-1tt**	−174.284232	0.31
propylcarbamic acid	−362.784720	**Pr-2tg**	−362.784248	0.30
butylamine	−213.546914	**Bu-1tgt**	−213.546154	0.48
butylcarbamic acid	−402.046920	**Bu-2ttt**	−402.046143	0.49
	$^{W}G_{298}$		$\langle ^{W}G_{298}\rangle$	$\langle ^{W}G_{rel}\rangle$
CO$_2$	−188.490145			
methylamine	−95.750847	**Me-1**		0.00
methylcarbamic acid	−284.251285	**Me-2**	−284.251083	0.13
ethylamine	−135.017565	**Et-1t**	−135.017138	0.27
ethylcarbamic acid	−323.516394	**Et-2t**	−323.516174	0.14
propylamine	−174.279509	**Pr-1tt**	−174.279018	0.31
propylcarbamic acid	−362.779142	**Pr-2tg**	−362.778672	0.29
butylamine	−213.541563	**Bu-1tgt**	−213.540802	0.48
butylcarbamic acid	−402.0412611	**Bu-2ttt**	−402.040484	0.49

[a]G_{298} and $\langle G_{298}\rangle$ in Hartree, $\langle G_{rel}\rangle$ in kcal/mol. [b]Values computed with Wertz correction indicated by superscript "W".

described the process to obtain all possible trial structures for the ethyl systems, and the same protocol was followed for the propyl and butyl systems. For these larger systems, the numbers of possible structures grow quickly, and Newman projections of the conformations of propylamine and of propylcarbamic acid are therefore enumerated using Schemes S2 and S3. For brevity, we will only show the more stable 2-type structures of the carbamic acids while the 3-type structures are included in the Supporting Information. We will proceed for the butyl systems in the same way.

As with ethylamine, the first letter describes the conformation about the N−C1 bond. The extension of the carbon skeleton requires one more label to describe the conformation about the C1−C2 bond, i.e., the dihedral angle τ = $\angle$(N−C1−C2−C3). There are at most three possibilities for the relative orientation between the terminal CH$_3$ group and the amino group. The Newman projections on the top row of Scheme S2 are derivatives of **Et-1t**, and in **Pr-1tt**, the terminal methyl group is *trans* with regard to the NH$_2$ group. The other isomers have the terminal CH$_3$ group in one of two *gauche* positions, and for these conformations, we use the labels **g** ($\tau \approx$ −60°) and **q** ($\tau \approx$ +60°). Note that **Pr-1tg** and **Pr-1tq** are enantiomeric structures, and the latter equals **Pr-1tg'**. In the bottom row of Scheme S2 are shown the derivatives of **Et-1g**, and the three structures **Pr-1gg**, **Pr-1gt**, and **Pr-1gq** are unique and asymmetric rotamer structures.

Replacement of H$_a$ with a carboxyl group in the structures of propylamine in the first row of Scheme S2 affords the carbamic acid structures in the first row of Scheme S3. In contrast to **Pr-1**, all three structures **Pr-2tg**, **Pr-2tt**, and **Pr-2tq** are unique asymmetric structures. Replacement of either H$_b$ or H$_a$ in the structures of propylamine in the second row of Scheme S2 affords the carbamic acid structures on the second and third rows of Scheme S3. However, because of the N-planarization, some of the **Pr-2c** and **Pr-2h** structures are not unique. For example, **Pr-2cg** and **Pr-2cq** would be enantiomeric structures, and the same with **Pr-2hg** and **Pr-2hq**. Overall, we expected up to seven unique structures of **Pr-2** and, in addition, an equal number of unique structures of **Pr-3**. However, not all of these structures correspond to stationary structures on the potential energy surface.

3.2.2. Models of Local Minima of Propylamine and Propylcarbamic Acid. Overall, one needs to search for five unique structures of propylamine **Pr-1** and nine local minima enter the Boltzmann analysis. All five structures were located (Figure 3).

The structures **Pr-2t** and **Pr-2c** are shown in Figure 4. Except for **Pr-2ct**, all of these structures are local minima. In Figure S4, structures of types **Pr-3t** and **Pr-3c** are shown, and except for **Pr-3ct**, all of these were also local minima. As in the

Table 4. Thermochemistry of the Carbamylation Reactions[a,b,c,d]

carbamylation reaction	ΔE	ΔH	$\Delta(T\cdot S)$	$\Delta(T\cdot^{W}S)$	ΔG_{MSS}	$\Delta^{W}G_{MSS}$	ΔA_{MSS}	$\Delta^{W}A_{MSS}$	$\Delta G_{MSS} - \Delta^{W}G_{MSS}$	$\Delta G_{MSS} - \Delta^{W}A_{MSS}$
R0: **Me-1** + CO$_2$ → **Me-2**	−14.81	−13.43	−9.76	−6.97	−3.67	−6.46	−3.08	−5.87	2.79	2.20
R1: **Et-1t** + CO$_2$ → **Et-2t**	−14.59	−13.10	−10.53	−7.65	−2.57	−5.45	−1.98	−4.86	2.87	2.28
R2: **Pr-1tt** + CO$_2$ → **Pr-2tg**	−14.94	−13.39	−10.36	−7.44	−3.03	−5.95	−2.44	−5.36	2.92	2.33
R3: **Bu-1tgt** + CO$_2$ → **Bu-2ttt**	−14.76	−13.27	−10.24	−7.28	−3.03	−6.00	−2.44	−5.40	2.96	2.36
average (R0:R3)	−14.77	−13.30	−10.22	−7.34	−3.08	−5.96	−2.49	−5.37	2.89	2.29
Stdev.P (R0:R3)	0.12	0.13	0.28	0.25	0.39	0.36	0.39	0.36	0.06	0.06
	ΔE_{BD}	ΔH_{BD}	$\Delta(T\cdot S_{BD})$	$\Delta(T\cdot^{W}S_{BD})$	ΔG_{BD}	$\Delta^{W}G_{BD}$	ΔA_{BD}	$\Delta^{W}A_{BD}$	$\Delta G_{BD} - \Delta^{W}G_{BD}$	$\Delta G_{BD} - \Delta^{W}A_{BD}$
R0: **Me-1** + CO$_2$ → **Me-2/3**	−14.65	−13.13	−9.59	−6.80	−3.54	−6.33	−2.95	−5.74	2.79	2.20
R1: **Et-1** + CO$_2$ → **Et-2/3**	−14.72	−13.19	−10.48	−7.61	−2.70	−5.58	−2.11	−4.99	2.87	2.28
R2: **Pr-1** + CO$_2$ → **Pr-2/3**	−15.04	−13.34	−10.30	−7.38	−3.04	−5.97	−2.45	−5.37	2.92	2.33
R3: **Bu-1** + CO$_2$ → **Bu-2/3**	−15.25	−13.46	−10.43	−7.47	−3.02	−5.98	−2.43	−5.39	2.96	2.36
average (R0:R3)	−14.91	−13.28	−10.20	−7.32	−3.08	−5.97	−2.49	−5.37	2.89	2.29
Stdev.P (R0:R3)	0.24	0.13	0.36	0.31	0.30	0.27	0.30	0.27	0.06	0.06

[a]Reaction energies of the carbamylation reactions in kcal/mol. Reaction entropy terms $\Delta(T\cdot S)$ computed for room temperature. [b]ΔG_{MSS} values are Gibbs reaction enthalpies based on the most stable structures of substrates and products. [c]Reaction energies that include the Wertz correction for solution translational entropy indicated by superscript "W". [d]Helmholtz data computed based on $\Delta^{W}G$ with pV correction.

Figure 3. Optimized structures of propylamine conformers. The number in parentheses is the population percentage in the Boltzmann analysis at 298 K for a single unique enantiomeric conformer. Note that the combined populations of **Pr-1tg** and its enantiomeric conformer **Pr-1tg′** greatly exceed the population of the all-*trans* structure.
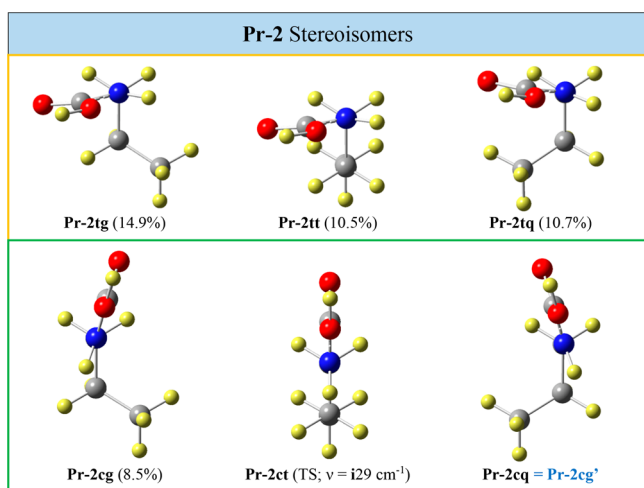
Figure 4. Optimized structures of propylcarbamic acid **Pr-2**. The number in parentheses is the population percentage in the Boltzmann analysis at 298 K for a single unique enantiomeric conformer.

case of the ethyl system, none of the **Pr-Xh** conformations could be located. In **Pr-2c** and **Pr-3c**, the planarization of the amide N occurs and the large COOH group at N must be staggered between the H atoms of the $C(1)H_2$ methylene group. These structures inadvertently contain one near-eclipsed C2−C1−N−H moiety. It is one consequence that **Pr-2cg** and **Pr-2cq** no longer represent different local minima because the enantiomeric conformer **Pr-2cg′** equals **Pr-2cq** (Figure 4); that is, the conformations about the C1−N and C1−C2 bonds are correlated in **Pr-2cg** and **Pr-2cq**. The same is true for **Pr-3cg** and **Pr-3cq**. In Table 1, we chose to list **Pr-2cg** and **Pr-3cg** with degeneracies of two, and **Pr-2cq** and **Pr-3cq** are not considered in the Boltzmann analysis. There will be similar cases in the following section, and we will apply this convention throughout.

None of the structures **Pr-2h** and **Pr-3h** exist as local minima, and no structures of these types appear in Figure 4 or Figure S4. The planarization at the amide N would place the large COOH group in an eclipsed conformation about the C1−N bond, $\chi \approx 0°$. We happened to locate the C_s-symmetric

structure **Pr-2ht**, and it is a transition-state structure ($\nu = \mathbf{i}103$ cm^{-1}) for rotation about the C1−N bond. The energy and structural data for **Pr-2ht** are included in the Supporting Information.

We located four unique asymmetric structures for **Pr-2** and four unique asymmetric structures and one unique symmetric structure for **Pr-3**. For the reasons given above, the symmetric structure, **Pr-3ct**, was not considered in the Boltzmann analysis. All of the asymmetric structures have enantiomeric conformers, so that a total of 16 conformers of propylcarbamic acid were considered in the Boltzmann analysis.

3.2.3. Potential Energy Surface for PrNH−COOH Torsion. As with ethylamine, we investigated the rotation about the dihedral angle $\chi = \angle(HO_2C−N−C1−C2)$, which connects the propylcarbamic acid structures with C_s symmetry, namely, **Pr-2ct** and **Pr-3ct**, to the structures of type **Pr-2tt** and **Pr-3tt**, respectively. The results were very similar to those of the ethylamine case. The **Pr-2ct** region is very flat, as shown in Figure 5. The C_s-symmetric "transition state" is slightly more pronounced, and the sinks for the surrounding C_1-local "minima", **Pr-2ct**(C_1) and **Pr-2ct′**(C_1), are slightly deeper than those for the ethyl system. Still, they are much too shallow to be considered bound minima, and therefore, **Pr-2ct**(C_1) and its enantiomeric conformer are UBMs. In fact, all attempts to locate the minima with the topology of **Pr-2ct** using initial structures with small distortions from the C_s-structure led to a structure of the **Pr-2tt**-type. The **Pr-2ct** region is simply a transition-state region for the interconversion between enantiomeric conformers **Pr-2tt** ⇌ **Pr-2tt′**.

Again, similar to the ethylamine case, the C_s-symmetric **Pr-3ct** is a shallow local minimum on the PES ($\nu_1 = 35$ cm^{-1}) and the barrier to rotation about the N−C1 bond is only $\Delta E = 0.36$ kcal/mol. This value is lower than the thermal energy associated with the ν_1 mode of the stationary structure **Pr-3ct** (0.594 kcal/mol). Thus, the stationary structure **Pr-3ct** is also a UBM and therefore not considered in the Boltzmann analysis. Essentially, the entire **Pr-3c** region is a transition-state region for the interconversion between enantiomeric conformers **Pr-3tt** ⇌ **Pr-3tt′**.

The sinks around **Pr-2tt** and **Pr-2tt′** are shallow and contain at most two bound vibrational states for the normal mode promoting the rotation about the C1−N bond ($\nu_3 = 101$ cm^{-1}). The sinks around **Pr-3tt** and its enantiomeric conformer are also shallow, containing at most two bound vibrational states for the normal mode promoting the rotation about the C1−N bond ($\nu_3 = 96$ cm^{-1}). Therefore, **Pr-2** is a fluxional molecule with equal populations of **Pr-2tt** and **Pr-2tt′**, and **Pr-3** is also a fluxional molecule with equal populations of **Pr-3tt** and **Pr-3tt′**.

3.2.4. Relative Energies and Population Analysis. The all-*trans* **Pr-1tt** is the most stable structure as expected. Yet, the *gauche* structure **Pr-1tg** with $\tau = \angle(N−C1−C2−C3) \approx 60°$ is nearly isoenergetic, and because it comes with an enantiomeric conformer, *gauche* structures dominate. Structures of the **Pr-1g**-type are all significantly higher in energy but still account for about 13% of the population.

For the propylcarbamic acids, structures with a *gauche* conformation with respect to the C1−C2 bond dominate. **Pr-2tg** is the most stable structure, and it is preferred by about 0.2 kcal/mol over the fully *trans* structure. **Pr-2tq** is virtually isoenergetic with **Pr-2tt**. The *gauche* preference persists even when the carbamino group is rotated such that the COOH group is staggered between H_c and H_d and **Pr-2cg**, and its
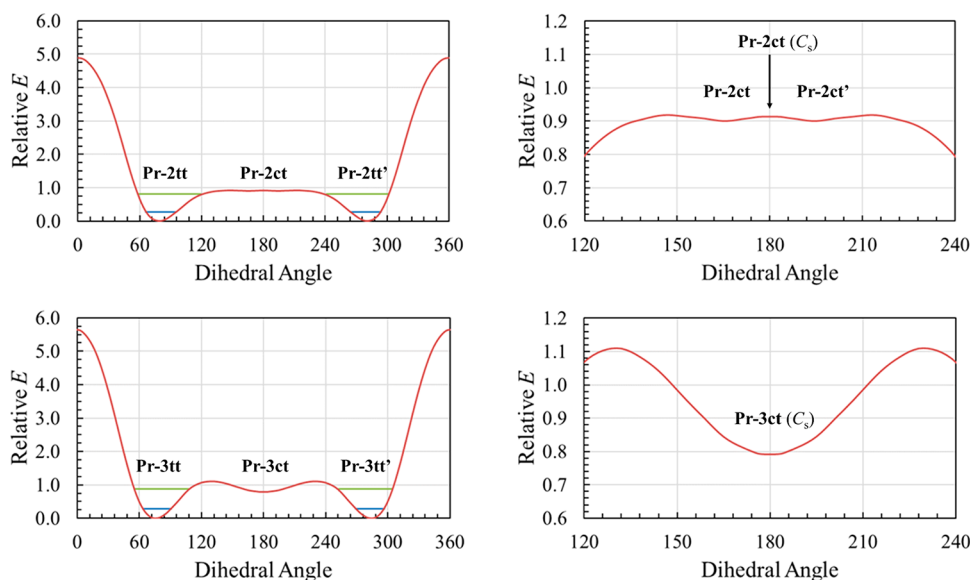
Figure 5. PES scans of the dihedral angle $\chi = \angle(HO_2C-N-C1-C2)$ for propylcarbamic acids **Pr-2** and **Pr-3**. Plots on the left show the full χ range and plots on the right are close-ups of the regions containing **Pr-2c** and **Pr-3c**, respectively. Relative energy E in kcal/mol. See caption to Figure 2.

enantiomeric conformer are the only structures of that type with large contributions to the overall propylcarbamic acid population. In general, we found a strong preference for the conformations with the *trans*-amide bond over the *cis*-amide bond; that is, **Pr-2** is generally preferred over **Pr-3**. The stability difference of the *trans*- and *cis*-amides is large enough that all of the **Pr-3** structures combined only account for 11% of the propylcarbamic acid population.

As **Pr-1tt** and **Pr-2tg** are the most stable structures, they are included in Table 3. Averaging over all nine propylamine minima, the average energy of propylamine at room temperature is increased by 0.31 kcal/mol from its most stable structure. Averaging over all 16 propylcarbamic acids, the energy is increased by 0.30 kcal/mol from its most stable structure. Both averaged molecules have increased energies of approximately the same amount such that the thermochemistry of the reaction using the Boltzmann averages is virtually unchanged from the thermochemistry using the most stable structures (Table 4). Put another way, because both the propylamine and the propylcarbamic acid have several available low-lying minima, the distributions of the molecules are readily able to adjust to temperature, and therefore, the energy available at room temperature is easily tolerated by a simple change in the species distributions for both molecules.

3.3. Enumeration of Conformations of Butylamine and *N*-Butylcarbamic Acid. 3.3.1. Possible Structures. The investigated conformers of butylamine are shown in Scheme S4. For the butyl systems, an extra label is required to distinguish the conformations. As before, the first label refers to the conformation about the N−C1 bond, and the second label refers to the conformation about the C1−C2 bond. The third and new label describes the conformation about the C2−C3 bond, and the structures shown feature dihedral angles $\phi = \angle(C1-C2-C3-C4)$ that are either *trans* (**t**, $\phi \approx 180°$) or *gauche* (**g**, $\phi \approx -60°$; **q**, $\phi \approx +60°$). Each butylamine conformation can be thought of as a derivative of a propylamine, where one of the terminal H atoms is replaced by a methyl group. Thus, there are three butylamine conformations for every parent propylamine conformer. In

Scheme S4, the first two descriptions are the same in each row (i.e., **Bu-1tg** in row 1, **Bu-1tt** in row 2, etc.). Of course, not all of the conformations are unique, and more pairs of enantiomeric conformers are expected for the butyl system. For example, the extension of the carbon chains of the pair of enantiomeric conformers **Pr-1tg** (row 1) and **Pr-1tq** (row 3) does not lead to six new and unique trial structures because **Bu-1tqg = Bu-1tgq′**, **Bu-1tqq = Bu-1tgg′**, **Bu-1tqt = Bu-1tgt′**. In such cases, we always consider the trial structure that appears first in the scheme. Total, we expect up to 14 unique structures of butylamine, one symmetric conformation (**Bu-1ttt**) and 13 asymmetric conformations, which would yield a maximum of 27 conformers for the Boltzmann statistical analysis.

The top three rows of the butylcarbamic acid trial structures in Scheme S5 correspond to the butylamine structures in Scheme S4, where H_a has been replaced by COOH. All nine of the **Bu-2t**-type structures are unique and asymmetric. Replacement of H_b or H_a in the **Bu-1g**-type structures with COOH yields nine trial structures of **Bu-2c** and nine structures of **Bu-2h**. Further, we expected the same number of conformations and with the same symmetry for the **Bu-3t**, **Bu-3c**, and **Bu-3h** trial structures. Thus, there are 27 unique trial structures for each of **Bu-2** and **Bu-3** (Table 1).

3.3.2. Models of Local Minima of Butylamine and *N*-Butylcarbamic Acid. All 14 unique structures of butylamine were located, and they are shown in Figure 6. For butylcarbamic acid, not all of these putative conformations correspond to stationary structures. The molecular models of the conformers that do exist as local minima on the potential energy surface for **Bu-2** are shown in Figure 7 and for **Bu-3** in Figure S5.

None of the **Bu-2h** conformations could be located as stationary structures because of steric problems between the COOH group and the C2 methylene group in any structure with $\chi \approx 0°$. Only three structures of the **Bu-2c** conformations ($\chi \approx 180°$) could be located as unique minima, but many of the **Bu-2c**-type trial structures would rotate about χ during optimization and yield structures of the **Bu-2t**-type. Attempts
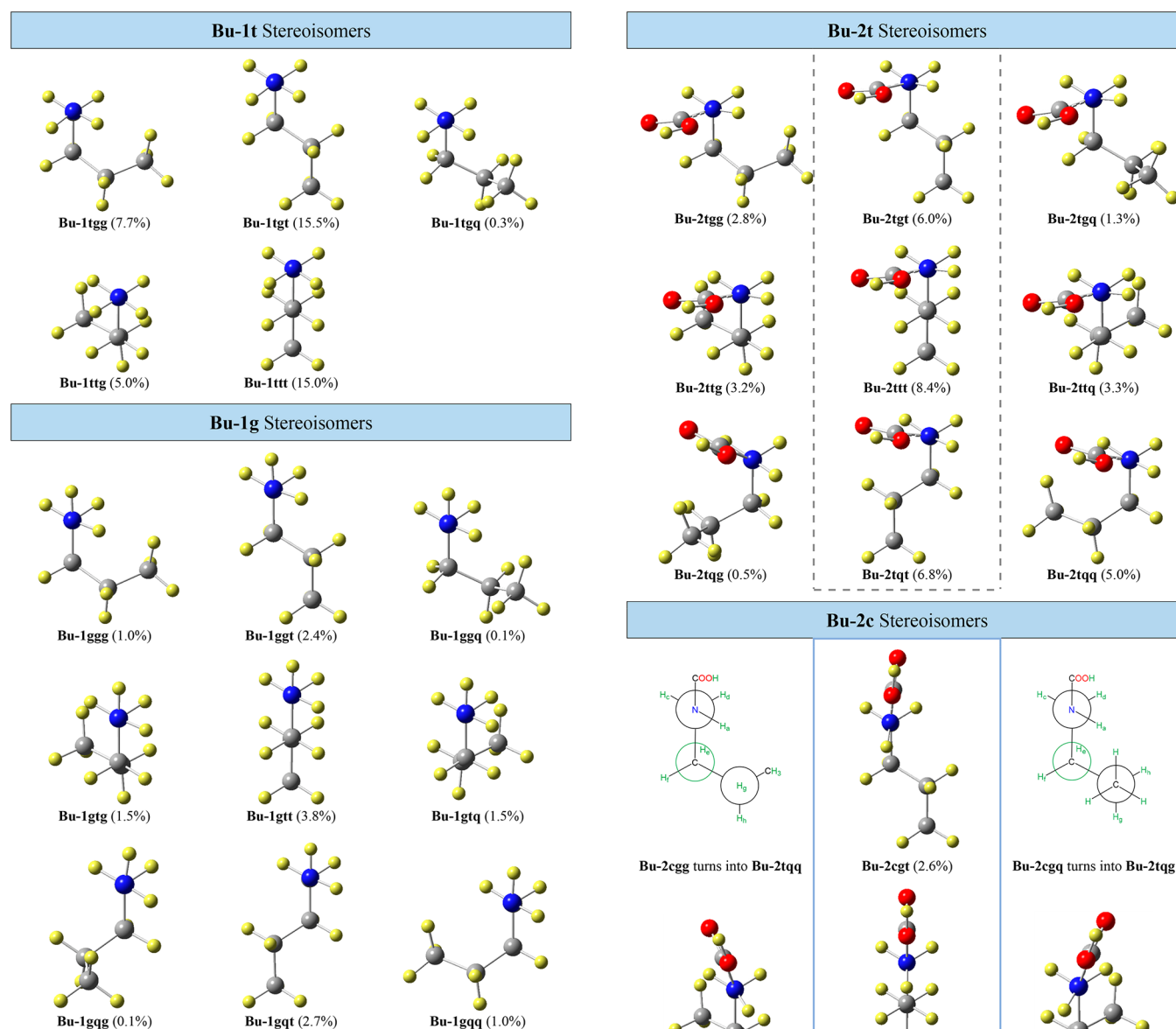
Figure 6. Optimized structures of butylamine conformers **Bu-1t** (top) and **Bu-1g** (bottom). Population numbers appearing as in previous figures. Again, the **t**-type structures dominate, even though there are many more **g**-type conformations.

to locate a structure of type **Bu-2cgg**, for example, led to the minimum of type **Bu-2tqq**. As with the propyl systems, in some types of trial structures, the dihedral angles about the C1−N and the C1−C2 bonds are correlated, and we deal with these situations in the same way as before. For example, we recognize that the structure **Bu-2ctq** is the mirror image of **Bu-2ctg**, and hence, we consider the enantiomeric conformers **Bu-2ctg** and **Bu-2ctg′** (but not **Bu-2ctq** and **Bu-2ctq′**). The same is true for structure types **Bu-2cgt** and **Bu-2cqt**.

Interestingly, all **Bu-3t** and **Bu-3c** structures were found to exist as local minima, except for **Bu-3ctt**, which of course is a transition state. As with the ethyl and propyl systems, these *cis*-amides are generally less stable than the analogous *trans*-amides (**Bu-2**). As with the **Bu-2t** structures, the most stable **Bu-3t** structures are those with the *trans* configuration about the C2−C3 bond ($\phi \approx 180°$).

3.3.3. Potential Energy Surface for BuNH−COOH Torsion. We also computed the C_s-structure for **Bu-2ctt**, and it is a
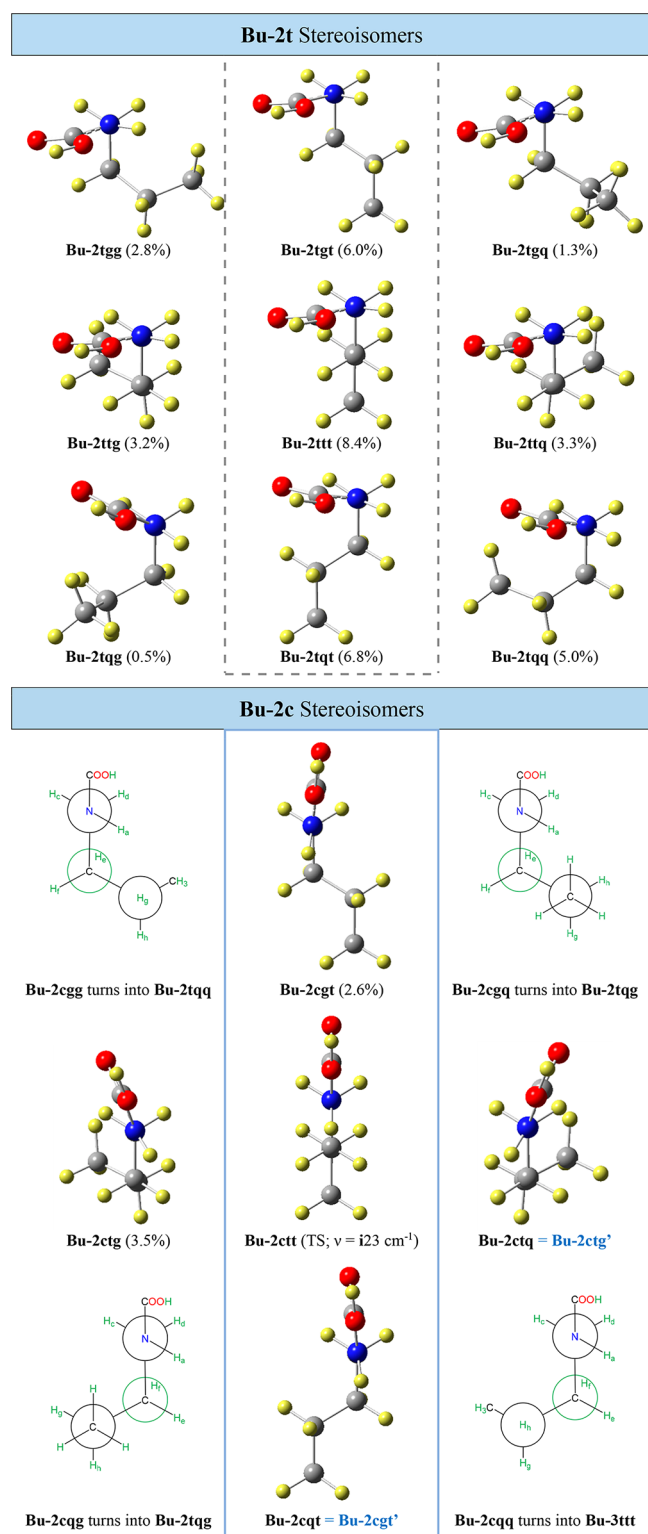
Figure 7. Optimized structures of the **Bu-2t**-type and **Bu-2c**-type of butylcarbamic acid conformers.

"transition-state" structure (ν_1 = **i**23.47 cm^{-1}). Since the barrier between C_s-**Bu-2ctt** and the adjacent pair of enantiomeric conformers **Bu-2ctt**(C_1) and **Bu-2ctt′**(C_1) is tiny, this region corresponds to one fluxional structure of type **Bu-2ctt**. Moreover, the rotational barrier between this **Bu-2ctt** region and the adjacent slightly more stable local minimum **Bu-2ttt** also is very low (Figure 8), and thus, the fluxional
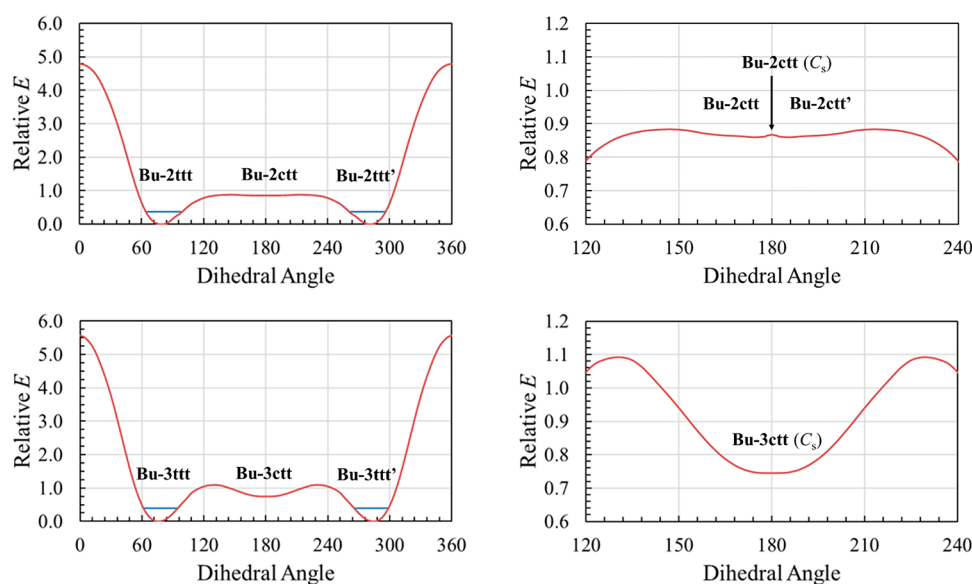
Figure 8. PES scans of the dihedral angle $\chi = \angle(HO_2C-N-C1-C2)$ for the propylcarbamic acids **Bu-2** and **Bu-3**. Plots on the left show the full χ range and plots on the right are close-ups of the regions containing **Bu-2c** and **Bu-3c**. Relative E in kcal/mol. See caption of Figure 2 for details.

structures of type **Bu-2ctt** are merely tiny bumps in the transition-state region for the interconversion between enantiomeric conformers **Bu-2ttt** ⇆ **Bu-2ttt′**.

In Table 5, our best estimates are summarized of the activation barriers for the interconversions between enantio-

Table 5. Activation Barriers for the Interconversions between Enantiomeric Conformers of Et-2t, Pr-2tt, and Bu-2ttt[a]

M	C_s, TS	ΔE	ΔH	$\Delta(T \cdot S)$	ΔG_{MSS}	ΔG_{BD}
Et-2t	**Et-2c**	0.73	0.04	−0.85	0.89	0.75
Pr-2tt	**Pr-2ct**	0.92	0.19	−0.75	0.93	0.85
Bu-2ttt	**Bu-2ctt**	0.83	0.17	−0.94	1.11	0.62

[a]All values in kcal/mol.

meric conformers **R-2t** ⇆ **R-2t′** of the most stable **R-2t** conformers (R = Et, Pr, Bu) by rotation about the $RH_2C-NH(CO_2H)$ bond via the transition-state structures with $\chi = \angle(C2-C1-N-COOH) = 180°$. The activation energies ΔG_{MSS} values are close to 1 kcal/mol. The average energy of the carbamic acids are higher than the energy of the minima **R-2t** because of the Boltzmann distribution, the activation energies ΔG_{BD} in column of Table 5 account for this effect, and they further lower the barriers to less than 0.9 kcal/mol.

3.3.4. Relative Energies and Population Analysis. All of the unique butylamine trial structures exist as local minima on the potential energy surface. Of the **Bu-1t** structures, the most stable are **Bu-1tgt** and **Bu-1ttt**, where $\phi \approx 180°$, and they are nearly isoenergetic. **Bu-1tgg** and **Bu-1ttg** are also present in significant amounts at 298 K. **Bu-1tgq**, however, is much higher in energy and has very little contribution to the overall population. The **Bu-1t** structures are generally favored over the **Bu-1g** structures. With the **Bu-1g** structures, we again found that the structures with $\phi \approx 180°$ are the lowest in energy and **Bu-1gtt** is slightly more favored than **Bu-1ggt** and **Bu-1gqt**. **Bu-1gtg** and **Bu-1gtq**, where $\phi = -60°$, $+60°$, respectively, are the almost isoenergetic and have the next highest contribution and are only slightly preferred over **Bu-1ggg** and **Bu-1gqq**, which also have $\tau = -60°$, $+60°$, respectively. **Bu-1ggq** and **Bu-**

1gqg are the highest energy structures and have very low contributions to the overall population.

All of the **Bu-2t** conformers exist as stationary structures and are shown in the top three rows of Figure 7. The **Bu-2t** structures with a *trans* conformation about the C2−C3 bond ($\phi \approx 180°$) are noticeably more stable than those conformers that have ϕ *gauche*. The most stable structure is **Bu-2ttt**, which accounts for 8.4% of the overall population, and **Bu-2tgt** and **Bu-2tqt** account for 6.0 and 6.8%, respectively. Most of the structures that are *gauche* with respect to ϕ are essentially isoenergetic, and each contribute roughly 3% to the total population with three exceptions. Two exceptions, **Bu-2tgq** and **Bu-2tqg**, have the terminal methyl group and the COOH group oriented in the same direction, which is sterically disfavored, and therefore, they account for only 1.3 and 0.5% of the total population, respectively. The third exception, **Bu-2tqq**, is more stable than the others and accounts for 5.0% of the total population. The only **Bu-2c**-type structures found to be stationary structures were **Bu-2cgt** and **Bu-2ctg**; they also have relatively high energy and together account for only 6.1% of the overall population.

The **Bu-3**-type structures are shown in Figure S5 and totally contribute only 7.5% to the overall population. The relative stabilities of the **Bu-3**-type structures follow the same pattern as the **Bu-2**-type structures. The most stable of the **Bu-3**-type structures is **Bu-3ttt**, which contributes only 1.5% to the total population. The **Bu-3** structures that did not have an analogous **Bu-2** structure, namely, **Bu-3cgg** and **Bu-3cgq**, and their enantiomeric conformers are very high in energy and so have very little contribution to the Boltzmann analysis.

Table 3 lists the Gibbs free energies for the most stable structures of butylamine and butylcarbamic acid, **Bu-1tgt** and **Bu-2ttt**, respectively. Table 3 also includes the statistically averaged free energies of these molecules, and the relative energy difference. The reaction free energies for R3 are given in the final row of Table 3 for each approximation. Because both the reactants and the products of the reaction are offset by about 0.49 kcal/mol, the reaction thermochemistry is mostly unchanged for this system when using the Boltzmann analysis.
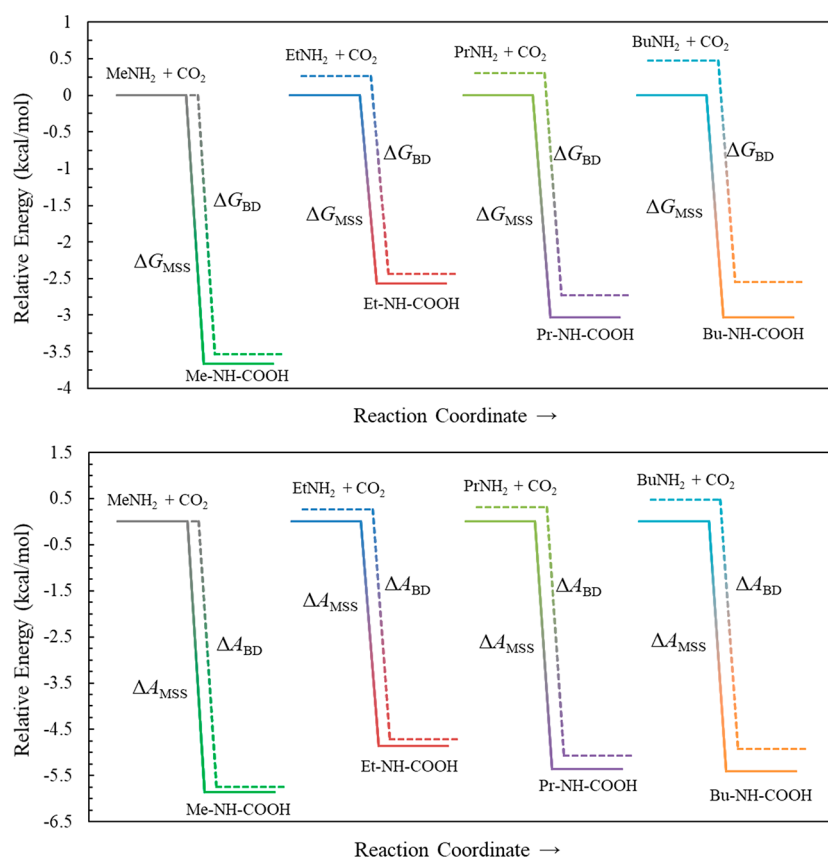
Figure 9. Reaction energy diagrams for the addition of CO_2 to methyl-, ethyl-, propyl-, and butylamine, highlighting the energy differences between the calculated ΔG (top) and ΔA (bottom) values with Wertz correction calculated using only the most stable structures and those calculated with the full ensemble using Boltzmann statistics.

3.4. Thermochemistry of the Carbamylation Reactions and Carbamic Acid Isomerizations. *3.4.1. Capture Reaction and Pareto Plots.* Figure 9 illustrates the main message of the computed data of Table 4. The solid lines correspond to the MSS model, and the dashed lines give the free energies $G_{rel}(M)$ and $A_{rel}(M)$ calculated with the Boltzmann statistical analysis for the amine (M = AM) and the carbamic acid (M = CA). Figure 9 shows that an increase in the number of accessible conformers increases the average energy of each system by $\langle G_{rel}(M) \rangle$. While it is obvious that the $\langle G_{rel}(M) \rangle$ values of amine and carbamic acid should increase, the estimation of that increase is unclear a priori, and moreover, it is also not clear how these increases affect reaction energies ΔG and the statistical contribution SC = ΔG_{MSS} − ΔG_{BD} = $\langle G_{rel}(AM) \rangle$ − $\langle G_{rel}(CA) \rangle$.

For the methyl systems $\langle G_{rel}(MeNH_2) \rangle$ = 0 kcal/mol and $\langle G_{rel}(MeNHCOOH) \rangle$ = 0.13 kcal/mol (Table 3), the statistical correction for the carbamylation of the methylamine is negative, SC = −0.13 kcal/mol. In contrast, the ethyl system $\langle G_{rel}(EtNH_2) \rangle$ is not zero, and in fact, $\langle G_{rel}(EtNH_2) \rangle$ = 0.27 kcal/mol is *larger* than $\langle G_{rel}(EtNHCOOH) \rangle$ = 0.14 kcal/mol (Table 3), so that SC becomes positive with SC = +0.13 kcal/mol. Figure 9 shows the qualitatively expected increase of the $\langle G_{rel}(M) \rangle$ values for propyl and butyl systems. Unexpected and perhaps also surprising is our finding that the SC values for the propyl (0.01 kcal/mol) and butyl systems (−0.01 kcal/mol) are practically negligible. This conclusion is also true for Helmholtz free energies ΔA_{BD} and ΔA_{MSS}, as shown in Figure 9 (bottom).

Pareto plots were generated to illustrate the distribution of species in conformational space (Figure 10). A Pareto plot includes a column graph of the percent contribution of each conformer plotted by decreasing significance on the horizontal axis. The plot also includes a Pareto line that keeps a running total of percentage of conformational space covered by the conformations to the left. In each plot, the range of the primary axis was selected for best resolution, and the secondary axis was added for the Pareto line. Most chemists tend to assume that $\langle G_{rel}(M) \rangle$ is somehow related to the number of accessible conformations of M and that the statistical correction, SC, might be related to the difference of accessible conformations of substrate and product. Yet, this assumption is not even true to a first approximation. If Figure 10 shows anything, it is that the origin of $\langle G_{rel}(M) \rangle$ is intractable. No matter how hard one tries, there is no short-cut to a reasonable estimate of SC. Thus, the most important conclusions to take away from the present study are that $G_{rel}(M)$ is modest for every molecule and that SC is entirely negligible at room temperature for the propyl and butyl systems.

For a given molecule, the effect of the Wertz correction on the molecular translational entropy is the same so that $\langle G_{rel} \rangle$ = $\langle {}^W G_{rel} \rangle$. The combined effect of the proper accounting for the molecular translation entropies in solution reduces the free energy of the capture reactions by $\langle \Delta G_{BD} - \Delta^W G_{BD} \rangle$ = 2.89 ± 0.06 kcal/mol.

The free energies $\Delta^W G$ include pV terms and lead to a more exothermic capture reaction merely because the number of molecules is reduced. However, we are interested in the
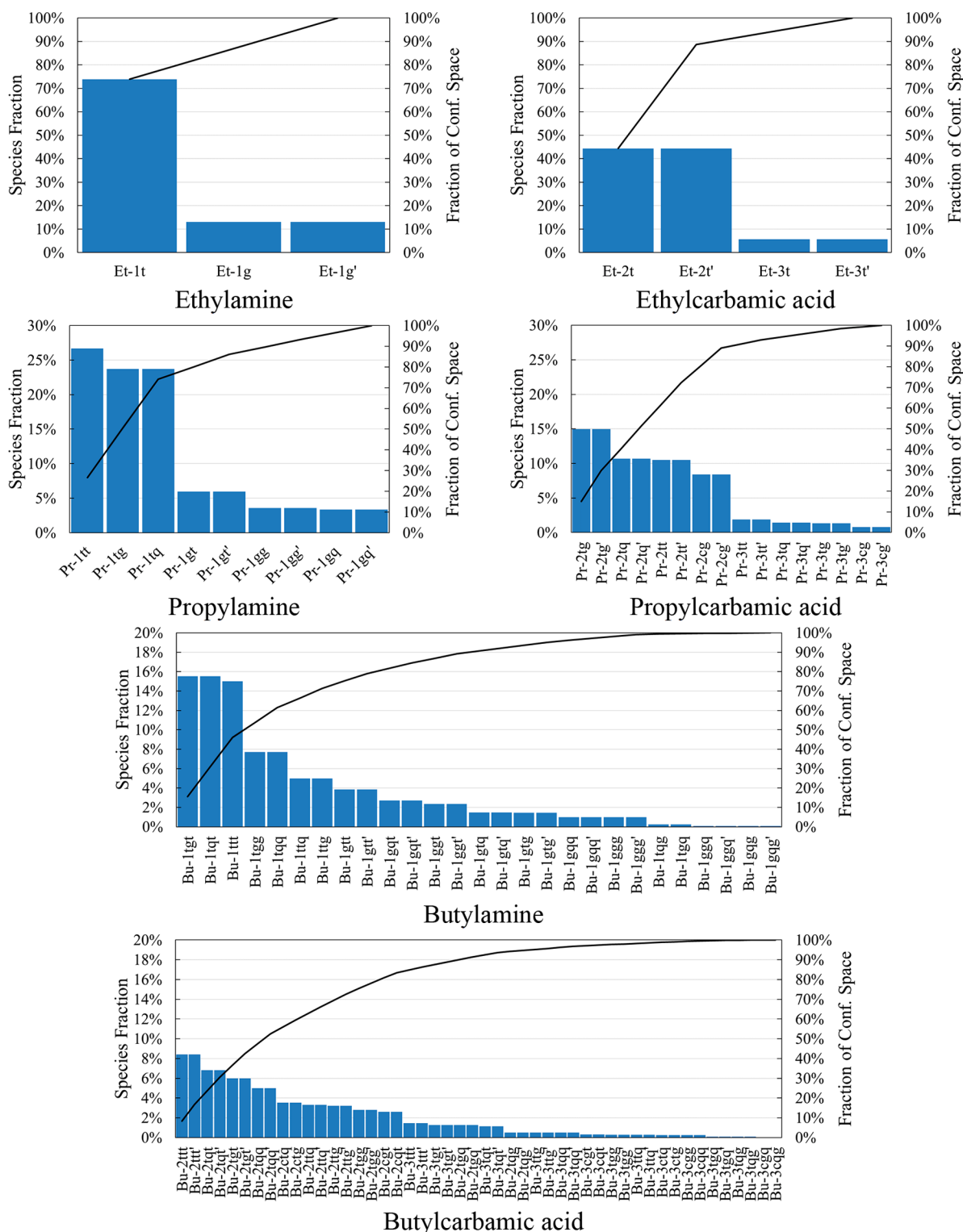
Figure 10. Pareto plots showing the relative contributions of each conformer of alkylamines **R-1** and carbamic acids **R-2** and **R-3** (R = Et, Pr, Bu).

capture reaction *in solution*, and the Helmholtz free energy $\Delta^W A$ is physically more meaningful because it does not include the pV term. The $\Delta^W A_{BD}$ values are more negative than the ΔG_{BD} values of the capture reactions (Table 4) by an average of $\langle \Delta G_{BD} - \Delta^W A_{BD} \rangle = 2.29 \pm 0.06$ kcal/mol. These $\Delta^W A_{BD}$ values are our best estimates for the carbamylation reactions in aqueous solution. Clearly, to compute best estimates of the capture reaction in solution, it is far more important to

consider translational entropy and volume effects than it is to sample the entire conformational space of each molecule. The Helmholtz reaction energies $\Delta^W A_{BD}$ depend only slightly on the nature of the alkyl group with $\langle \Delta^W A_{BD} \rangle = -5.37 \pm 0.27$ kcal/mol, the variation is not steady, and there is practically no change going from propyl to butyl systems.

3.4.2. Activation Barrier for the Face-Change Isomerization of Carbamic Acids. In the mechanistic discussion of

Figure 11. Rotational profiles of **Pr-2t** and **Bu-2t** with regard to their ∠(N−C1−C2−C3) dihedral angles (°) to explore the isomerization that causes the face change of the carbamate group relative to the [C1,C2,C3] plane. For **Pr-2c** and **Bu-2c**, only the most relevant stationary structures are included.

Rubisco carbamylation, the question becomes relevant as to the facility of the migration of the carbamate functional group from one face of the alkyl chain to the other. This question can be explored here with studies of the rotational profiles of the propyl and the butyl systems (Figure 11). In Table 6, we

Table 6. Activation Barrier of Face Change[a,b]

minimum	TS	ΔE	ΔH	$\Delta(T{\cdot}S)$	ΔG_{MSS}	ΔG_{BD}
Pr-2tg	**Pr-2TS1**	4.08	3.59	−1.45	5.04	4.75
Pr-2tg	**Pr-2TS2**	3.78	3.21	−1.15	4.36	4.07
Pr-2tg	**Pr-2TS3**	3.40	2.84	−1.21	4.05	3.75
Pr-2tg	**Pr-2TS4**	4.67	4.17	−0.56	4.73	4.43
Bu-2ttt	**Bu-2TS1**	3.88	3.50	−1.63	5.13	4.65
Bu-2ttt	**Bu-2TS2**	2.99	2.49	−1.52	4.01	3.52
Bu-2ttt	**Bu-2TS3**	3.39	2.77	−1.13	3.89	3.41
Bu-2ttt	**Bu-2TS4**	4.29	3.86	−0.77	4.63	4.14

[a]Activation energies in kcal/mol. [b]In every row, all values are based on the most stable minimum structure on the ΔG surface.

provide activation energies, and all of those are relative to the most stable minimum on the ΔG surfaces (**Pr-2tg**, **Bu-2ttt**). For isomerizations, the translational entropies and the pV terms are invariant, and we provide activation energies ΔG_{MSS} and ΔG_{BD}. The following discussion focus on ΔG_{MSS} data.

The face change is accomplished in the propyl system by way of rotation about the (Me)H$_2$C−CH$_2$NH(CO$_2$H) bond, and inspection of Figure 4 shows that there are two potential pathways. The rotation can be accomplished while maintaining the **Pr-2t** conformation (Figure 4, first row) or the rotation might proceed with **Pr-2c** conformation (Figure 4, second row). Therefore, we calculated the rotational profile about that bond in the **Pr-2t** conformation (Figure 11, solid orange line) and located all three rotational transition-state structures **Pr-2TS1**, **Pr-2TS2**, and **Pr-2TS3**. The direct one-step conversion **Pr-2tg** − (**Pr-2TS1**) − **Pr-2tq** leads to steric interference between the terminal methyl group and the carbamic acid moiety and requires ΔG_{MSS} = 5.0 kcal/mol. The best way to convert **Pr-2tg** to **Pr-2tq** involves rotation in the opposite direction via **Pr-2tt**; **Pr-2tg** − (**Pr-2TS2**) − **Pr-2tt** − (**Pr-**

2TS3) − **Pr-2tq**, and the highest activation barrier along this path is ΔG_{MSS} = 4.4 kcal/mol.

We also scanned the respective rotational profile for the **Pr-2c** conformation. Rotation of the methyl group starting at **Pr-2cg** led to the transition-state **Pr-2TS4** (Figure 11, solid green line) and after further rotation to **Pr-2tt**-type structures with the rotational profile merging into the orange profile. Similarly, rotation starting at **Pr-2cq** leads to **Pr-2TS5** in a symmetrically related path. The rotational profile shows relative energies and suggests that **TS4** is above **TS1**. However, on the ΔG surface, **TS4** is more stable than **TS1** but remains less stable than **TS2**.

For the butyl system, the face change of the carbamate group with regard to the [C1,C2,C3] plane again requires rotation of the C3 carbon about the C1−C2 bond (MeH$_2$C)H$_2$C−CH$_2$NH(CO$_2$H). There are more options in the butyl case because C3 carries a methyl group, and we studied the case with C2−C3 *trans* conformation in analogy to the study of the propyl system (Figure 11). As with the propyl system, we studied the interconversion of **Bu-2tgt** to **Bu-2tqt** both directly via **Bu-2TS1** and indirectly via **Bu-2TS2** and **Bu-2TS3** (Figure 11, dashed gray line). We also studied the interconversion for the **Bu-2c** conformation (Figure 11, blue line). In contrast to the propyl case, **Bu-2ct** can be reached without collapsing to the **Bu-2ttt**. The barriers for the three isomerization paths follow the same order as with the propyl systems, and the lowest activation barrier for the butyl system is ΔG_{MSS} = 4.0 kcal/mol.

The availability of the large conformational spaces for the propyl- and butylcarbamic acids actually reduce the activation barriers for face change isomerization. The average energy of the carbamic acid is higher than the energy of the most stable minimum. The last column in Table 6 lists the activation energies ΔG_{BD}, which account for this effect. For the propyl system, the isomerization barrier is reduced from ΔG_{MSS} = 4.36 kcal/mol to ΔG_{BD} = 4.07 kcal/mol, and for the butyl systems, the reduction is from ΔG_{MSS} = 4.01 kcal/mol to ΔG_{BD} = 3.52 kcal/mol. The more pronounced effect for the butyl system is a direct consequence of $\langle G_{rel} \rangle$ increasing with the size of the alkyl group (Table 2).

4. CONCLUSION

The present work provides a solid foundation for our experimental studies of the CO_2 capture reactions because of the application of an accurate solvation model for the potential energy surface analyses at the level SMD(APFD/6-311G*), the consideration of the full conformational spaces of amine and carbamic acid in Boltzmann analysis, and the proper accounting for translational entropy and volume effects in solution.

Of all the possible structures, two (out of two) unique conformers of ethylamine, four (out of six) unique conformers of ethylcarbamic acid, five (out of five) unique conformers of propylamine, nine (out of 18) unique conformers of propylcarbamic acid, 14 (out of 14) unique conformers of butylamine, and 26 (out of 54) unique conformers of butylcarbamic acid were found to exist as minima on the potential energy surfaces. Based on calculated energies of these structures, a population analysis was conducted using Boltzmann statistics at room temperature.

The interconversions between enantiomeric conformers **R-2t** ⇋ **R-2t′** of the most stable **R-2t** conformers (R = Et, Pr, Bu) proceed by rotation about the $RH_2C-NH(CO_2H)$ bond via the transition-state structures with $\chi = \angle(R-C-N-C) = 180°$. The regions of the potential energy surfaces between the enantiomeric minima of the *trans*-carbamic acids **Et-2t** and **Et-2t′**, **Pr-2tt** and **Pr-2tt′**, and **Bu-2ttt** and **Bu-2ttt′** are topologically similar (Figures 2, 5, and 8). Though two very shallow minima and one transition state technically exist in each case, their contributions to the ensemble are negligible. For the interconversions between enantiomeric conformers **R-3t** ⇋ **R-3t′** of the *cis*-carbamic acids, the corresponding PES regions contain a more pronounced local minimum. However, these minima do not correspond to bound states at room temperature, and they were excluded from the Boltzmann ensemble.

We determined the reaction energies of the carbamylation reactions based on the traditional approach of considering just the most stable structures and based on the ensemble energies computed with the Boltzmann distribution. The difference between these approaches is small for R = Me and Et, and it is entirely negligible for the larger systems with R = Pr and Bu. The effect of the proper accounting for the molecular translational entropies in solution are much more significant and reduces the free energy of the capture reactions by $\langle \Delta G_{BD} - \Delta^W G_{BD} \rangle = 2.89 \pm 0.06$ kcal/mol: from $\langle \Delta G_{BD} \rangle = -3.08 \pm 0.30$ kcal/mol to $\langle \Delta^W G_{BD} \rangle = -5.97 \pm 0.27$ kcal/mol for all R groups and, for the butyl system, from $\langle \Delta G_{BD} \rangle = -3.02$ kcal/mol to $\langle \Delta^W G_{BD} \rangle = -5.98$ kcal/mol. Finally, accounting for volume effects in solution results in our best estimates for the reaction energies of the carbamylation reactions and give values of $\langle \Delta^W A_{BD} \rangle = -5.37 \pm 0.27$ kcal/mol for all R groups and of $\langle \Delta^W A_{BD} \rangle = -5.39$ kcal/mol for the butyl system.

■ ASSOCIATED CONTENT

Ⓢ Supporting Information

The Supporting Information is available free of charge at https://pubs.acs.org/doi/10.1021/acs.jpca.1c06294.

> Brief discussion of theoretical level dependency with focus on N-pyramidalization, Table S2 with the thermodynamic properties and relative energies of all carbamic acid structures, several schemes and figures related to the conformational space analyses, and Cartesian coordinates of all stationary structures determined at the SMD(APFD/6-311G*) level (PDF)

■ AUTHOR INFORMATION

Corresponding Author

Rainer Glaser − *Department of Chemistry, Missouri University of Science & Technology, Rolla, Missouri 65409, United States;* ⓘ orcid.org/0000-0003-3673-3858; Email: GlaserR@umsystem.edu

Authors

Joseph Schell − *Department of Chemistry, Missouri University of Science & Technology, Rolla, Missouri 65409, United States; Department of Chemistry, University of Missouri, Columbia, Missouri 65211, United States;* ⓘ orcid.org/0000-0001-8264-566X

Kaidi Yang − *Department of Chemistry, University of Missouri, Columbia, Missouri 65211, United States*

Complete contact information is available at:
https://pubs.acs.org/10.1021/acs.jpca.1c06294

Author Contributions

J.S. and K.Y. contributed equally to this work.

Notes

The authors declare no competing financial interest.

■ REFERENCES

(1) Trends in Atmospheric Carbon Dioxide, US Department of Commerce, National Oceanic & Atmospheric Administration (NOAA), Earth System Research Laboratory, Global Monitoring Division; http://www.esrl.noaa.gov/gmd/ccgg/trends/global.html (accessed on 2021-04-27).

(2) Smith, P.; Davis, S. J.; Creutzig, F.; Fuss, S.; Minx, J.; Gabrielle, B.; Kato, E.; Jackson, R. B.; Cowie, A.; Kriegler, E.; et al. Biophysical and Economic Limits to Negative CO_2 Emissions. *Nat. Clim. Change* **2016**, *6*, 42−50.

(3) Tollefson, J. Price of Sucking CO_2 from Air Plunges: Technology Moves Closer to Economic Viability. *Nature* **2018**, *558*, 173.

(4) Gutknecht, V.; Snæbjörnsdóttir, S. O.; Sigfússon, B.; Aradóttir, E. S.; Charles, L. Creating a Carbon Dioxide Removal Solution by Combining Rapid Mineralization of CO_2 with Direct Air Capture. *Energy Procedia* **2018**, *146*, 129−134.

(5) Fuss, S.; Canadell, J. G.; Peters, G. P.; Tavoni, M.; Andrew, R. M.; Ciais, P.; Jackson, R. B.; Jones, C. D.; Kraxner, F.; Nakicenovic, N.; et al. Betting on Negative Emissions. *Nat. Clim. Change* **2014**, *4*, 850−853.

(6) Wang, T.; Wang, X.; Hou, C.; Liu, J. Quaternary Functionalized Mesoporous Adsorbents for Ultra-high Kinetics of CO_2 Capture from Air. *Sci. Rep.* **2020**, *10*, 21429.

(7) Gislason, S. R.; Wolff-Boenisch, D.; Stefansson, A.; Oelkers, E. H.; Gunnlaugsson, E.; Sigurdardottir, H.; Sigfusson, B.; Broecker, W. S.; Matter, J. M.; Stute, M.; et al. Mineral Sequestration of Carbon Dioxide in Basalt: A Pre-Injection Overview of the CarbFix Project. *Int. J. Greenhouse Gas Control* **2010**, *4*, 537−545.

(8) Keith, D. W. Why Capture CO_2 from the Atmosphere? *Science* **2009**, *325*, 1654−1655.

(9) Solomon, S.; Plattner, G.-K.; Knutti, R.; Friedlingstein, P. Irreversible Climate Change Due to Carbon Dioxide Emissions. *Proc. Natl. Acad. Sci. U. S. A.* **2009**, *106*, 1704−1709.

(10) Hansen, J.; Sato, M.; Kharecha, P.; von Schuckmann, K.; Beerling, D. J.; Cao, J.; Marcott, S.; Masson-Delmotte, V.; Prather, M.

J.; Rohling, E. J.; et al. Young People's Burden: Requirement of Negative CO₂ Emissions. *Earth Syst. Dynam.* **2017**, *8*, 577−616.

(11) National Academies of Sciences, Engineering, and Medicine. *Negative Emissions Technologies and Reliable Sequestration: A Research Agenda*; The National Academies Press: Washington, DC, 2019; DOI: 10.17226/25259 (accessed on 2021-04-27).

(12) Kim, L. J.; Siegelman, R. L.; Jiang, H. Z. H.; Forse, A. C.; Lee, J. H.; Martell, J. D.; Milner, P. J.; Falkowski, J. M.; Neaton, J. B.; Reimer, J. A.; et al. Cooperative Carbon Capture and Steam Regeneration with Tetraamine-Appended Metal-Organic Frameworks. *Science* **2020**, *24*, 369−392.

(13) Yang, X.; Rees, R. J.; Conway, W.; Puxty, G.; Yang, Q.; Winkler, D. A. Computational Modeling and Simulation of CO₂ Capture by Aqueous Amines. *Chem. Rev.* **2017**, *117*, 9524−9593.

(14) National Academies of Sciences, Engineering, and Medicine. *Gaseous Carbon Waste Streams Utilization: Status and Research Needs*; The National Academies Press: Washington, DC, 2019; DOI: 10.17226/25232 (accessed on 2021-04-27).

(15) Hepburn, C.; Adlen, E.; Beddington, J.; Carter, E. A.; Fuss, S.; Mac Dowell, N.; Minx, J. C.; Smith, P.; Williams, C. K. The Technological and Economic Prospects for CO₂ Utilization and Removal. *Nature* **2019**, *575*, 87−97.

(16) Sanz-Perez, E. S.; Murdock, C. R.; Didas, S. A.; Jones, C. W. Direct Capture of CO₂ from Ambient Air. *Chem. Rev.* **2016**, *116*, 11840−11876.

(17) Canadell, J. G.; Monteiro, P. M. S.; Costa, M. H.; Cotrim da Cunha, L.; Cox, P. M.; Eliseev, A. V.; Henson, S.; Ishii, M.; Jaccard, S.; et al. 2021: Global Carbon and other Biogeochemical Cycles and Feedbacks. In *Climate Change 2021: The Physical Science Basis. Contribution of Working Group I to the Sixth Assessment Report of the Intergovernmental Panel on Climate Change*; Masson-Delmotte, V., Zhai, P., Pirani, A., Connors, S. L., Péan, C., Berger, S., Caud, N., Chen, Y., Goldfarb, L., Gomis, M. I., Eds.; Cambridge University Press, in press.

(18) McQueen, N.; Gomes, K. V.; McCormick, C.; Blumanthal, K.; Pisciotta, M.; Wilcox, J. A Review of Direct Air Capture (DAC): Scaling up Commercial Technologies and Innovating for the Future. *Prog. Energy* **2021**, *3*, 032001.

(19) Muelleman, A.; Schell, J.; Glazer, S.; Glaser, R. Thermochemistry of a Biomimetic and Rubisco-Inspired CO₂ Capture System from Air. *C − Journal of Carbon Research* **2016**, *2*, 18.

(20) Glaser, R. RuBisCO-Inspired Biomimetic Approaches to Reversible CO₂ Capture from Air. Metal Dependence of the H₂O/CO₂ Replacement Penalty. In *Advances in CO₂ Capture, Sequestration and Conversion*; Jin, F., He, L.-N., Hu, Y. H., Eds.; ACS Symposium Series; American Chemical Society: Washington, DC, 2015; Chapter 11, pp 265−293.

(21) Glaser, R.; Castello-Blindt, P. O.; Yin, J. Biomimetic Approaches to Reversible CO₂ Capture from Air. N-Methylcarbamic Acid Formation in Rubisco-Inspired Models. In *New and Future Developments in Catalysis, Activation of Carbon Dioxide*; Suib, S. L., Ed.; Elsevier 2013; Chapter 17, pp 501−534.

(22) Feller, U.; Anders, I.; Mae, T. Rubiscolytics: Fate of Rubisco after its Enzymatic Function in a Cell is Terminated. *J. Exp. Bot.* **2007**, *59*, 1615−1624.

(23) Taylor, T. C.; Andersson, I. Structure of a Product Complex of Spinach Ribulose-1,5-bisphosphate Carboxylase/Oxygenase. *Biochemistry* **1997**, *36*, 4041−4046.

(24) Cleland, W. W.; Andrews, T. J.; Gutteridge, S.; Hartman, F. C.; Lorimer, G. H. Mechanism of Rubisco: The Carbamate as General Base. *Chem. Rev.* **1998**, *98*, 549−561.

(25) Lorimer, G. H.; Badger, M. R.; Andrews, T. J. The Activation of Ribulose-1,5-bisphosphate Carboxylase by Carbon Dioxide and Magnesium Ions. Equilibria, Kinetics, a Suggested Mechanism, and Physiological Implications. *Biochemistry* **1976**, *15*, 529−536.

(26) Frisch, M. J.; Trucks, G. W.; Schlegel, H. B.; Scuseria, G. E.; Robb, M. A.; Cheeseman, J. R.; Scalmani, G.; Barone, V.; Petersson, G. A.; Nakatsuji, H.; et al. *Gaussian 16*, revision A.03; Gaussian, Inc.: Wallingford, CT, 2016.

(27) Austin, A.; Petersson, G.; Frisch, M. J.; Dobek, J.; Scalmani, G.; Throssell, K. A Density Functional with Spherical Atom Dispersion Terms. *J. Chem. Theory Comput.* **2012**, *8*, 4989−5007.

(28) Mclean, A. D.; Chandler, G. S. Contracted Gaussian Basis Sets for Molecular Calculations 1. 2nd Row Atoms, Z = 11−18. *J. Chem. Phys.* **1980**, *72*, 5639−5648.

(29) Krishnan, R.; Binkley, J. S.; Seeger, R.; Pople, J. A. Self-Consistent Molecular Orbital Methods 20. Basis Set for Correlated Wave-Functions. *J. Chem. Phys.* **1980**, *72*, 650−654.

(30) Frisch, M. J.; Pople, A.; Binkley, J. S. Self-Consistent Molecular Orbital Methods 25. Supplementary Functions for Gaussian Basis Sets. *J. Chem. Phys.* **1984**, *80*, 3265−3269.

(31) Marenich, A. V.; Cramer, C. J.; Truhlar, D. G. Universal Solvation Model Based on Solute Electron Density and on a Continuum Model of the Solvent Defined by the Bulk Dielectric Constant and Atomic Surface Tensions. *J. Phys. Chem. B* **2009**, *113*, 6378−6396.

(32) Medvedev, M. G.; Bushmarinov, I. S.; Sun, J.; Perdew, J. P.; Lyssenko, K. A. Density Functional Theory is Straying from the Path toward the Exact Functional. *Science* **2017**, *355*, 49−52.

(33) Bakowies, D.; von Lilienfeld, O. A. Density Functional Geometries and Zero-Point Energies in *Ab Initio* Thermochemical Treatments of Compounds with First-Row Atoms (H, C, N, O, F). *J. Chem. Theory Comput.* **2021**, *17*, 4872−4890.

(34) Sure, R.; Brandenburg, J. G.; Grimme, S. Small Atomic Orbital Basis Set First-Principles Quantum Chemical Methods for Large Molecular and Periodic Systems: A Critical Analysis of Error Sources. *ChemistryOpen* **2016**, *5*, 94−109.

(35) Balabin, R. M. Enthalpy Difference between Conformations of Normal Alkanes: Intramolecular Basis Set Superposition Error (BSSE) in the Case of *n*-Butane and *n*-Hexane. *J. Chem. Phys.* **2008**, *129*, 164101.

(36) Wertz, D. H. Relationship Between the Gas-phase Entropies of Molecules and their Entropies of Solvation in Water and 1-Octanol. *J. Am. Chem. Soc.* **1980**, *102*, 5316−5322.

(37) Darkhalil, I. D.; Nagels, N.; Herrebout, W. A.; van der Veken, B. J.; Gurusinghe, R. M.; Tubergen, M. J.; Durig, J. R. Microwave Spectra and Conformational Studies of Ethylamine from Temperature Dependent Raman Spectra of Xenon Solutions and Ab Initio Calculation. *J. Mol. Struct.* **2014**, *1068*, 101−111.